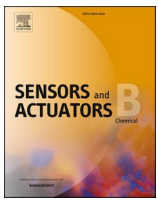
Sensors & Actuators: B. Chemical 379 (2023) 133248



Contents lists available at ScienceDirect

Sensors and Actuators: B. Chemical

journal homepage: www.elsevier.com/locate/snb





Construction of hierarchical porous 3D nanostructures with high specificity as SERS aptasensors for rapid and ultrasensitive detection of MC-LR

Qian Xie [a,1], Jinxin Chi [a,1], Zhixin Li [b], Xucong Lin [b], Guihua Huang [a,*]

[a] Institute of Analytical Technology and Smart Instruments, Xiamen Key Laboratory of Food and Drug Safety, College of Environment and Public Health, Xiamen Huaxia University, Xiamen 361024, China
[b] Institute of Food Safety and Environment Monitoring, Fuzhou University, Fuzhou 350108, China

ARTICLE INFO

Keywords:
Surface-enhanced Raman scattering
Aptasensors
Porous 3D nanostructures
High specific and ultrasensitive
Rapid detection

ABSTRACT

The construction of plasmonic nanostructures is a frontier research area in the field of Surface enhanced Raman scattering (SERS). Three-dimensional (3D) porous materials coupled with aptamers have attracted increasing attention for application in SERS sensing, owing to their great promise towards offering both high specific and ultrasensitive detection capacity. However, most of these SERS sensors are plane-shaped or solution-based, which makes target molecules with a reduced mass transfer, thus leading to a relatively poor capture efficiency. Herein, we demonstrate a capillary-based porous nanostructure coupled with aptamers that can serve as a type of SERS aptasensor for rapid trace detection. The aptasensor was prepared by immobilization of aptamer-modified SERS nanotags on a porous silica monolith which was obtained by an in-situ polymerization in a capillary with a facile fabrication process. The 3D porous silica monolith (3D-PSM) with a hierarchical biporous structure that could enable the rapid permeation of the aqueous phase and provide high specific surface area and active sites, endows the material with high capture efficiency of target molecules. Besides, according to the size of aptamers, stable and uniformed hotspots of 7–8 nm in size were formed, which precisely guaranteed the sensitivity, specificity, and stability of detection. The experimental verification showed that the proposed aptasensor could detect the presence of microcystin-LR at concentrations as low as 0.01 nmol/L, with fast recognition time (10 min), low sample consumption (20 μL), and simple operation. All the results suggest that this new strategy has promising potential in rapid microvolume trace analysis in various fields.

1. Introduction

Surface enhanced Raman scattering (SERS) is a powerful analytical technique for detecting trace-level molecules due to its rare advantage of providing intrinsic molecular fingerprint specificity with single-molecular sensitivity [1–3], and it has been widely applied in areas ranging from food safety, environmental monitoring and biomedical analysis [4–6]. The construction of plasmonic nanostructures on the substrates is highly critical in the field of SERS, because the normally weak Raman signals of analytes need to be amplified through the excitation of the localized surface plasmon resonance (LSPR) in plasmonic nanoparticles[7]. One of the most attractive strategies is to construct solid-based 3D plasmonic nanostructures that could provide a large number of “hot spots” (sub-10 nm narrow gap structures) [5,8–11]. Nevertheless, it is worth noting that most of the reported 3D SERS substrates are noble metal-based, and thus they face great challenges regarding how the target molecules to be enriched and captured in the “hot spot” regions [2]. Furthermore, the spacing distance of plasmonic nanoparticles within 10 nm is hard to control. On the other hand, commonly used solution-based metallic sol substrates also accompany issues such as poor reproducibility and position-dependent variation of signal intensity, owing to the instability of metallic colloid aggregates [8,12].

Recently, porous materials such as metal-organic frameworks (MOFs) [1,13], porous silica [5,14], gels [15] have been emerging as powerful nanostructures for developing SERS substrates due to their ultrahigh specific surface areas, significant structural flexibility and functionalizable pore interiors. However, it must be emphasized that most of these porous materials usually act as scaffolds for noble metal nanoparticles, and thus the obtained SERS substrates face challenges

* Corresponding author.
E-mail address: huanggh@hxxy.edu.cn (G. Huang).
[1] These authors contributed equally to this work.

https://doi.org/10.1016/j.snb.2022.133248
Received 31 October 2022; Received in revised form 15 December 2022; Accepted 25 December 2022
Available online 27 December 2022
0925-4005/© 2022 Published by Elsevier B.V.

pertaining to their lack of specificity towards target molecules. Aptamers are short single-stranded DNA (ssDNA) or RNA sequences, which can bind to the targets with high specificity and affinity [16]. Compared with antibodies, aptamers that offer significant advantages in terms of relatively small size, ease of synthesis and further functionalization, are more suitable for SERS sensing applications [17]. The introduction of functional aptamers on the porous nanostructures can increase the specific adsorption in the pores, improving the SERS detection specificity and sensitivity. Nevertheless, it is noted that most of the reported aptamer-based 3D porous SERS substrates are plane-shaped or used by dispersing the porous materials in an aqueous environment [18–20], and thus, the target molecules adsorb onto the surface of the substrates through mass transfer with a relatively poor capture efficiency, which leads to much longer detection time requirements, otherwise the Raman signal would be extremely weak.

Accordingly, the capillary-based porous 3D materials (capillary monoliths) are desirable sensor nanostructures to overcome these limitations and thus improving SERS sensing performance. The monolith characterized with ordered hierarchical meso-macroporous structures possesses the following advantages [5,21,22]: (I) the mesopores providing a high specific surface area and active sites for analyte entrapping as well as offering short diffusion path lengths, which can significantly improve the capture efficiency and reduce the analysis time; (II) the macroporosity enabling the rapid permeation of the aqueous phase; (III) the capillary structure being endowed with superiorities such as greatly reduced sample/reagent consumption, low cost mass production, and the ability to readily integrate into miniaturized systems, etc. The capillary monoliths have demonstrated considerable promise for SERS sensing applications owing to the combination of above-mentioned important properties [5,22]. Furthermore, the capillary-based porous 3D sensor can be used as a liquid flow channel and a detection chamber simultaneously. Target molecules could be effectively enriched and captured in the “hot spot” regions when liquid flow is pumped into the capillary channel. However, although these previously reported SERS substrates showed high detection sensitivity, rapid detection and simple operation, they still face the challenge of the lack of specificity in practical applications, and the construction of hotspots within 10 nm could not be flexibly designed and controlled.

Herein, we develop a capillary-based porous silica nanostructure coupled with aptamers as a high-performance SERS aptasensor for rapid, ultrasensitive and specific detection of trace microcystin-LR (MC-LR). MC-LR is the most toxic contaminant among microcystins. Human chronic exposure to low concentrations of MC-LR in drinking water can cause severe liver damage and even lead to liver cancer [23]. A regulatory limit of 1 μg/L (1 nM) for MC-LR in drinking water has been proposed by the World Health Organization (WHO) [24]. Thus, it is urgent to develop a specific and sensitive method for the rapid detection of trace levels of MC-LR. The 3D-PSM proposed here was fabricated by an in-situ polycondensation of siloxane in an ultraviolet transparent quartz capillary. Then, the 3D-PSM was functionalized with complementary DNA (cDNA) modified Au@Ag core-shell NPs following hybridization with SERS nanotags. The SERS nanotags prepared by immobilizing thiolated aptamers on Au@Ag core-shell NPs with Raman reporter of p-aminothiophenol (PATP) embedded were used for the detection. According to the chain length of cDNA, the stable and uniformed hotspots of 7–8 nm in size were formed between the tags and the Au@AgNPs immobilized on the surface of the 3D-PSM, which ensured the sensitivity, specificity, and stability of detection. The principle and procedure of the obtained aptamer-based 3D-PSM for SERS sensing of MC-LR are illustrated in Scheme 1. The developed 3D SERS aptasensor detection relied on the SERS signal-off response of PATP upon exposure to target molecules, which is due to the aptamer dissociated from the cDNA and consequently leading to the release of SERS nanotags from hybridized SERS-active 3D-PSM. The established new platform shows great potential in the rapid detection of trace amounts of toxins, and other field analysis of micro-volume complex samples including food safety, environmental monitoring and public health.

2. Materials and methods

2.1. Chemicals and materials

Quartz silica capillary (100 μm i.d. × 360 μm o.d.) was purchased from Yongnian optic fiber plant (Hebei, China). All reagents and solvents in analytical grade were purchased from commercial suppliers (Detail in S1). MC-LR aptamer, complementary DNA, control oligonucleotide and control oligonucleotide complementary DNA were fabricated and purified by Sangon Biotech. Co. (Shanghai, China). Sequence of Oligonucleotides was listed in Table S1. Crucian carps were purchased from the local supermarket. The binding buffer solution (BB) (Tris-HCl 10 mM, NaCl 120 mM, $CaCl_2$ 20 mM, KCl 5.0 mM) with pH 7.40 was prepared. Water was purified using a Milli-Q apparatus (Millipore, USA).

2.2. Synthesis of Au@AgNPs and Au@PATP@AgNPs

AuNPs with a diameter of 15 ± 2.0 nm were first synthesized according to our previously reported protocols [5], and the procedure for synthesization was described in S2.1. Then, to prepare the SERS nanotags, PATP as a Raman label was used to functionalize Au cores and the procedure for functionalization was described in S2.2. Finally, Au@Ag NPs and Au@PATP@Ag NPs were prepared and the procedure preparation was described in S2.2.

2.3. Immobilization of cDNA and aptamers

The cDNA and MC-LR aptamers were immobilized on Au@AgNPs and Au@PATP@AgNPs through the formation of Ag-S bonds, and consequently the Au@AgNPs@cDNA and Au@PATP@AgNPs@Aptamer (SERS-tag) were obtained respectively, as shown in Fig. 1. The detailed procedures for immobilization are described in S2.3.

2.4. Fabrication of 3D SERS aptasensor

The 3D SERS aptasensor was prepared based on a porous silica monolith with an inter-connected porous network structure. The porous silica monolith was fabricated by a one-pot process according to our previously reported protocols [5], and the optimal recipe was listed in Table S2. The polymerization solution was a homogeneous mixture composed of siloxane monomers (TEOS and AEAPTES) and porogen reagent system (ethanol, water and CTAB). The detailed fabrication process of this porous silica monolith was described in S2.4. The 3D SERS aptasensor was obtained via complementary base pairing of cDNA-conjugated Au@AgNPs and MC-LR aptamer-conjugated Au@PATP@AgNPs. The fabrication process of the 3D SERS aptasensor was described in S2.5.

2.5. Characterization

The characterization of the prepared NPs and 3D nanostructures was described in S3.

2.6. Detection of MC-LR

The stock solution of MC-LR was first diluted to obtain a series of standard solutions with different concentrations (0, 0.01, 0.05, 0.10, 0.50, 1.0, 5.0, 10.0, 50, and 100 nM), and the procedure for the detection of MC-LR was described in S4.1. The SERS spectra were obtained using a microscopic Raman spectrometer (ATR8300AF, Optosky, China) with a 20 × objective and a laser wavelength of 785 nm. The laser was focused on the center of the capillary. The detection parameters were listed in Table S3.

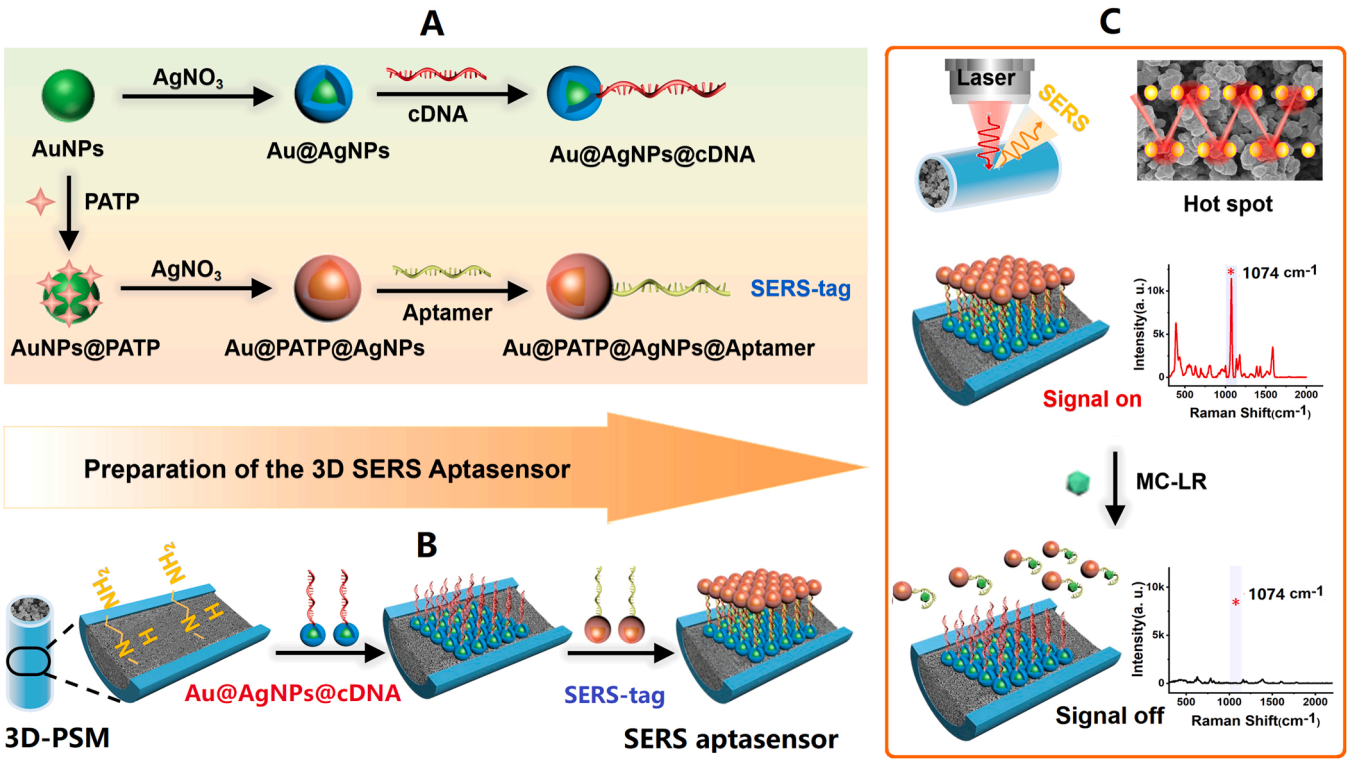


Fig. 1. Schematic demonstration of the fabrication of SERS aptasensor with 3D porous silica monolith (3D-PSM) for the detection of MC-LR.

2.7. Specificity evaluation

To evaluate the specificity of the proposed SERS aptasensor for MC-LR, the analogs of MC-LR, other common microcystins (MC-YR and MC-RR), as well as several mycotoxins (OTA, OTB and AFB1) were respectively detected by using this SERS aptasensor. Solvent blank was used as a negative control. Besides, a control ssDNA SERS sensor for detecting all of the above samples was also investigated.

2.8. Detection of real samples

The applicability of the proposed SERS aptasensors was evaluated for the detection of MC-LR in real samples such as tap-water and crucian carp. The tap-water samples were taken from our laboratory water pipe, and the preparation procedure was described in S4.2. Fresh live crucian carps were purchased from the local supermarket. The crucian carp samples were treated according to the previous reference [25], and the preparation procedure was described in S4.3. The procedures for SERS detection were the same as Section 2.6.

3. Results and discussion

3.1. Design strategy of the 3D SERS aptasensors for MC-LR detection

The mechanism of the proposed SERS aptsensor and sensing strategy for MC-LR detection was shown in Fig. 1. Two functionalized Au@Ag core-shell NPs of Au@AgNPs@cDNA and Au@PATP@AgNPs@Aptamer were used to create the aptasensors. The synthesis procedure was shown in Fig. 1A. Firstly, Au seed of approximately 15 nm was synthesized. And then, for the fabrication of Au@AgNPs@cDNA, Ag atoms were deposited directly on Au cores to form an Ag shell by reducing $AgNO_3$, whereas for the fabrication of Au@PATP@AgNPs@Aptamer (SERS tags), PATP was embedded in the junction of Au core and Ag shell. Subsequently, Au@AgNPs and Au@PATP@AgNPs were functionalized with thiolated cDNA and MC-LR aptamer through the formation of Ag-S bonds, respectively. The 3D-PSM was prepared by a one-pot process according to our previously reported protocols [5]. The Au@AgNPs@cDNA was pumped through the 3D-PSM and could be assembled on the surface amino groups of the 3D-PSM through electrostatic attraction. After that, the SERS tags were pumped through the 3D-PSM modified with Au@AgNPs@cDNA, and the tags could be captured on the 3D-PSM via hybridization chain reaction between aptamer-conjugated tags and cDNA, and therefore, the 3D SERS aptasensor platform was established (Fig. 1B). In the absence of MC-LR, the strong Raman signals from PATP could be detected because of the "hot spot" effect generated by the nano-gap between Au@AgNPs@cDNA and Au@PATP@AgNPs@Aptamer. As shown in Fig. 1C, in the presence of MC-LR, the aptamer SERS tags would dissociate from the cDNA due to the high affinity and specificity of MC-LR toward aptamers, resulting in a great decrease in the SERS signals of PATP after a washing step. According to the linear relationship between the logarithm of MC-LR concentration and SERS intensity of PATP, quantitative detection of MC-LR could be achieved using the proposed 3D SERS aptasensors.

3.2. Preparation and characterization of Au@AgNPs@cDNA and Au@PATP@AgNPs@Aptamer

As well-known, Au-Ag bimetallic core-shell nanostructures could provide a better SERS enhancement effect due to their unique plasmonic properties [26]. In this study, Au@Ag core-shell nanoparticles were prepared and used to be anchored on a porous silica monolith that possesses a large surface area with abundant amino groups, and therefore resulting in a stronger SERS enhancement. Besides that, the silver shell could protect the Raman signal of PATP from being affected by the external factors. Fig. 2A, C and E showed the transmission electron microscopy (TEM) images of AuNPs, Au@AgNPs and Au@PATP@AgNPs, respectively. The average diameter of AuNPs was 15 nm (Fig. 2A). The Au@AgNPs were attempted to be synthesized by the deposition of Ag atoms on surfaces of Au cores. As shown in Fig. 2C, the newly formed Ag atoms were closely and uniformly deposited on the surfaces of Au cores to generate Au@AgNPs. The average sizes of the Au@AgNPs were found to be 30 nm and the thickness of Ag shell was

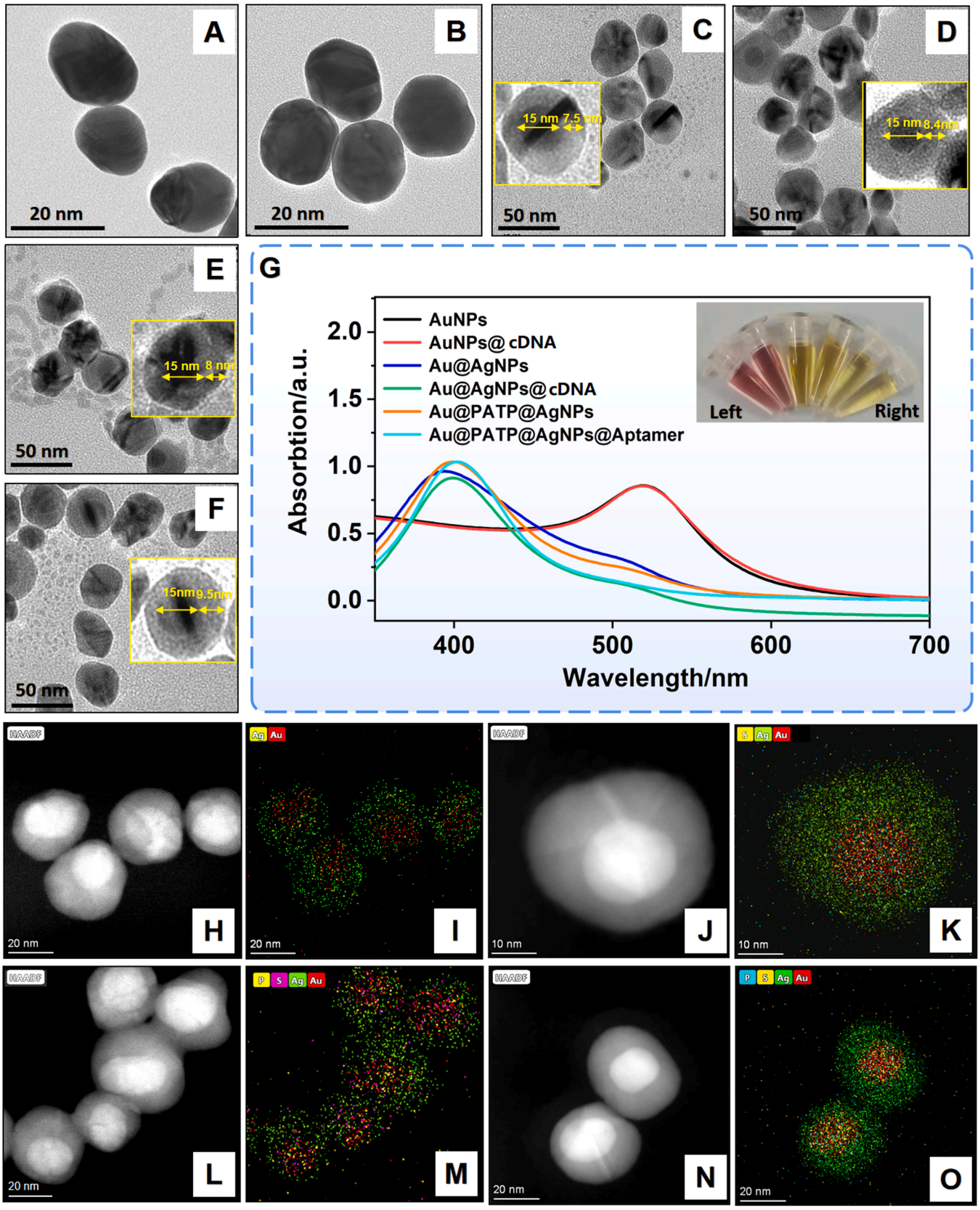


Fig. 2. Representative TEM images of AuNPs (A), Au@cDNA (B), Au@AgNPs (C), Au@AgNPs@cDNA (D), Au@PATP@AgNPs (E), and Au@PATP@AgNPs@Aptamer (F). The UV–vis spectra (G) of prepared AuNPs, Au@cDNA, Au@AgNPs, Au@AgNPs@cDNA, Au@PATP@AgNPs, and Au@PATP@AgNPs@Aptamer. Insert, from left to right in the photographs are AuNPs, Au@cDNA, Au@AgNPs, Au@AgNPs@cDNA, Au@PATP@AgNPs, and Au@PATP@AgNPs@Aptamer. Representative HAADF-STEM images and the corresponding elements mapping images of Au@AgNPs (H and I), Au@PATP@AgNPs (J and K), Au@AgNPs@cDNA (L and M), and Au@PATP@AgNPs@Aptamer (N and O).

about 7.5 nm (Fig. 2C). The PATP as Raman reporter was attached to the surface of the Au cores through the Au-S covalent bonds and then a layer of Ag atoms was deposited on the surface of Au@PATP to generate Au@PATP@AgNPs. The homogeneous and spherical morphology was still observed and the average sizes of the Au@PATP@AgNPs were approximately 31 nm and the thickness of PATP@Ag shell was about 8 nm (Fig. 2E).

The AuNPs, Au@AgNPs and Au@PATP@AgNPs were modified with cDNA and MC-LR aptamers through the formation of Ag-S bonds to obtain Au@cDNA, Au@AgNPs@cDNA and Au@PATP@AgNPs@Aptamer (SERS-tag). These NPs were characterized by TEM, UV-Vis, HAADF-STEM, TEM mapping and Zeta potential. As shown in Fig. S1, the Zeta potential of Au@AgNPs and Au@PATP@AgNPs were − 35.21 mV and − 35.91 mV respectively, which were mainly due to negative charged citrate ions on the surface of NPs [27]. However, after modification of cDNA and aptamers on the surface of Au@AgNPs and Au@PATP@AgNPs respectively, the Zeta potential of Au@AgNPs@cDNA and Au@PATP@AgNPs@Aptamer displayed more negative charge (−35.21 to −40.84 mV and −35.91 to −41.38 mV, respectively), owing to the negative charges of the phosphate groups on the cDNA/aptamer backbone in the aqueous solution. The optical properties of AuNPs, Au@cDNA, Au@AgNPs, Au@AgNPs@cDNA, Au@PATP@AgNPs and Au@PATP@AgNPs@Aptamer were recorded by UV-Vis absorption spectra. As shown in Fig. 2G, the AuNPs showed a wine red color with a unique UV-Vis absorption peak at 520 nm. After a layer of Ag atoms deposited on the surfaces of Au core, Au@AgNPs were generated and the solution color changed from wine red to orange. Simultaneously, a new UV-Vis absorption peak of the Ag shell appeared at 398 nm, which indicated the formation of Ag shell on the surfaces of Au cores [28]. Additionally, the UV-Vis absorption peaks of Au@cDNA (521 nm), Au@AgNPs@cDNA (401 nm) and Au@PATP@AgNPs@Aptamer (402 nm) were slightly red-shifted compared with that of AuNPs, Au@AgNPs and Au@PATP@AgNPs, which were mainly due to the change in the dielectric environment of the metal nanoparticles by the adsorption of cDNA or aptamers. This result was consistent with that of the reported literature [29]. Moreover, to further verify the formation of the structures of Au@AgNPs, Au@PATP@AgNPs, Au@AgNPs@cDNA and Au@PATP@AgNPs@Aptamer, these NPs were characterized by HAADF-STEM and TEM mapping. The representative HAADF-STEM images and the corresponding elements mapping images of these NPs were shown in Fig. 2 H-O. These images exhibit element distribution clearly, and the Au-Ag core-shell nanostructures could also be easily observed. These results were consistent with the characterization by the Zeta potential.

3.3. Preparation and characterization of the 3D SERS aptasensor

The proposed 3D SERS aptasensor was created based on a 3D-PSM. The 3D-PSM was prepared by polymerization of TEOS and AEAPTES via a one-pot process. Fig. 3A and B showed the scanning electron microscopy (SEM) images of the obtained 3D-PSM with different magnification times. The SEM images showed that the 3D-PSM had homogeneous porous morphology and was well attached to the inner wall of the quartz capillary. The 3D-PSM that possessed a unique hierarchically porous structure containing both macropores and mesopores could not only enable the rapid permeation of the aqueous phase (macropores) but also provide high specific surface area and active sites (mesopores). Hence, the abundant amino groups on the surface of the 3D-PSM could provide a large amount of electrostatic interaction sites for the self-assembly of Au@AgNPs@cDNA. As shown in Fig. 3D and E, the SEM images of the 3D-PSM modified with Au@AgNPs@cDNA clearly demonstrated that the nanoparticles of Au@AgNPs@cDNA were successfully attached and uniformly distributed on the surface of the 3D porous framework (as shown in Fig. 3E), whereas the morphological structure of the 3D-PSM remained intact (as shown in Fig. 3D). Fig. 3C and F showed the SERS spectra of the 3D-PSM and the 3D-PSM modified with Au@AgNPs@cDNA, respectively. Since there were no significant Raman bands in both of the SERS spectra between 390 and 2000 cm^{-1}, it demonstrated that no interference occurred during the SERS measurement of MC-LR.

Fig. 3G and H showed the SEM images of the 3D SERS aptasensor which was obtained via hybridization chain reaction between cDNA-conjugated Au@AgNPs immobilized on the 3D-PSM and MC-LR aptamer-conjugated Au@PATP@AgNPs (SERS tags) pumped through the 3D-PSM. Clearly seen in Fig. 3H, the NPs were also uniformly distributed on the surface of the 3D porous framework. Meanwhile, as shown in Fig. 3G, the surface morphology and hierarchically porous structure still remained intact. Besides, the appearance of the characterized vibration peaks of PATP in the SERS spectra of the 3D SERS aptasensor (as shown in Fig. 3I) indicated that SERS tags were successfully captured by the cDNA-conjugated Au@AgNPs immobilized on the 3D-PSM. Considering that the Raman peak at 1074 cm^{-1} showed the strongest intensity, it was regarded as the characteristic signal for MC-LR detection. That is, in the presence of MC-LR, owing to the high specificity and high affinity of aptamers toward targets[24,28], SERS tags would dissociate from the Au@AgNPs@cDNA, and therefore, a decrease in SERS intensity at peak 1074 cm^{-1} would be observed. As the spectra displayed in Fig. 3L, after a volume of 20 μL of MC-LR (0.50 nM) percolating through the 3D SERS aptasensor, an obvious decrease in the intensity of the Raman peak at 1074 cm^{-1} was observed. Meanwhile, no obvious change was found on the morphological structure of the 3D SERS aptasensor (as shown in Fig. 3J), and the residual NPs were still immobilized on the surface of the 3D porous framework (as shown in Fig. 3K).

By contrasting the property of the 3D SERS aptasensor proposed in this study with that of the conventional 2D planar substrate, our design of the 3D-PSM has potential as an excellent platform for the rapid detection of trace molecules. When using conventional planar substrates for SERS detection, the substrates were generally required to be immersed in large volumes of sample solutions and followed by a drying process [10,30,31], which would cause large sample consumption and be time-consuming. While using the 3D SERS aptasensor proposed here, only a volume of 20 μL of sample solution was needed for one SERS analysis, and meanwhile, it could be used for direct detection in liquids without any drying process. Moreover, the unique 3D porous silica network could provide more active sites and specific surface areas as well as offering short diffusion path lengths, which can significantly improve the capture efficiency and reduce the recognition time. Furthermore, it is well known that the prerequisite to enhancing Raman signals is the rational construction of hot spots and placing analyte molecules in these hot spots. The hot spots can be generated at the nanogaps (<10 nm) between adjacent nanoparticles or at the tips and edges of a noble metal surface [4,12,32]. Fig. 3M showed the hairpin structure of the hybridization products of aptamer-conjugated tags reaction with cDNA modified on the Au@AgNPs that immobilized on the 3D-PSM. Considering the lengths of the Ag-S bond (1.8 nm), carbon chain (0.5 nm), and 15 base pairs (5.1 nm) [33], the interparticle distance between the tags and the Au@AgNPs immobilized on the surface of the 3D-PSM with which it was assembled was estimated to be 7.4 nm (<10 nm). Therefore, the SERS signal of the tags would be significantly amplified. To further demonstrate that the Raman enhancement was mainly attributed to the plasmon coupling between the SERS tags and the Au@AuNPs immobilized on the surface of the 3D-PSM, the SERS spectra using the substrate of 3D-PSM, 3D-PSM modified with SERS tags and the SERS aptasensors were measured, as shown in Fig. S2. It can be seen that, no SERS signal was obtained when using 3D-PSM as a SERS substrate, and the characteristic peaks of PATP could be obviously observed when using 3D-PSM modified with SERS tags and the SERS aptasensors, while, a significantly higher SERS intensity of PATP was observed when using the SERS aptasensors. Besides, the hotspot size was optimized by constructing different sizes of hotspots (4.0, 5.7, 7.4 and 9.1 nm) through utilizing several cDNA sequences with different chain

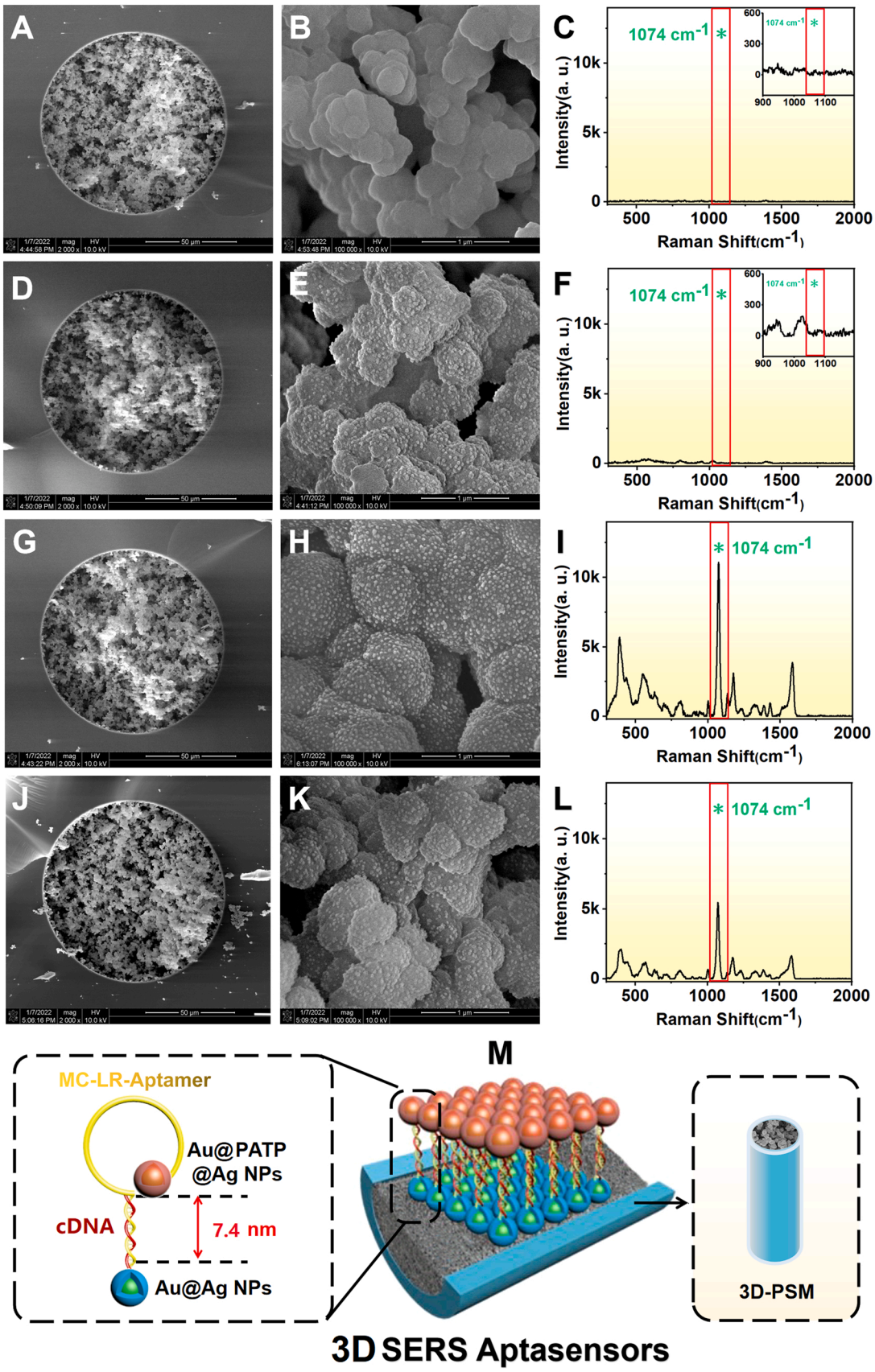


Fig. 3. Representative SEM images of the 3D-PSM (A:×2000, B:×100,000), 3D-PSM modified with Au@AgNPs@cDNA (D:×2000, E:×100,000), SERS aptasensor (G:×2000, H:×100,000) and SERS aptasensor after discrimination of MC-LR at concentrations of 0.5 nM (J:×2000, K:×100,000). SERS spectra of the 3D-PSM (C), 3D-PSM modified with Au@AgNPs@cDNA (F), SERS aptasensor (I) and SERS aptasensor after discrimination of MC-LR at concentrations of 0.5 nM (L). The hairpin structure of the hybridization products of cDNA reaction with aptamer-conjugated tags (M).

lengths (5, 10, 15 and 20 base pairs, as shown in Table S1). As shown in Fig. S3, the SERS signal increased with the increasing chain length of the cDNA sequence and the strongest SERS signal was observed when using the cDNA sequence with 15 base pairs (7–8 nm hotspot). This may be due to the fact that the DNA duplex stability is dependent on its length [34]. Nevertheless, the SERS signal decreased when using the cDNA sequence with more base pairs, such as 20 base pairs (9–10 nm hotspot). This may be owing to the decreased contribution of these hotspots to the SERS intensity. Therefore, the cDNA sequence with 15 base pairs was chosen to construct the SERS aptasensor. Meanwhile, due to the gap created between the Au@AgNPs and tags by using DNA as a linker, the gap was of the same size and stable, so that making the SERS-active nanostructures in a reproducible and uniform manner.

Compared to those 3D SERS aptasensor that decorated with AuNPs, here we recommend Au@Ag core-shell NPs as better SERS-active metallic nanostructures for generating SERS signal enhancements. We prepared the 3D-PSM decorated with AuNPs@cDNA and Au@AgNPs@cDNA respectively, while being hybridized with the same SERS tags. The SERS spectra of MC-LR at different concentrations (0, 0.1, 0.5, 1.0 nM) acquired from these two aptasensors were shown in Fig. S4. It could be found that the SERS signal intensity of the tags acquired from the aptasensor with Au@AgNPs@cDNA decorated showed evidently higher than that acquired from the aptasensor with AuNPs@cDNA decorated. This result indicated that the Au@Ag core-shell NPs could provide a better SERS enhancement effect. Therefore, the Au@Ag core-shell NPs were adopted to create the 3D SERS aptasensor.

Additionally, we fabricated the 3D SERS aptasensor through the hybridization chain reaction between aptamer-conjugated tags (Au@PATP@AgNPs@Aptamer) and cDNA modified on the 3D-PSM. And the Raman peak of PATP at 1074 cm^{-1} was regarded as the characteristic signal for MC-LR detection. Therefore, the amount of tags that directly affect the signal intensity of PATP should be carefully considered. Different volume of tags solution including 100 μL, 150 μL, 200 μL, 250 μL and 300 μL were pumped through the 3D-PSM modified with Au@AgNPs@cDNA. As shown in Fig. S5, the characteristic peaks at 1074 cm^{-1} could be clearly observed and the SERS intensity increased rapidly with increasing the volume of tags solution from 100 to 200 μL. However, when the volume of tags solution increased, for example, up to 250 μL, no significant change in the SERS intensity of PATP was observed, owing to the saturation effect of the tags. Therefore, the volume of tags solution of 200 μL was selected as an optimal volume for the fabrication of the 3D SERS aptasensor.

3.4. Detection of MC-LR standard solutions

The feasibility of the developed 3D SERS aptasensor for rapid detection of trace MC-LR was first studied by testing MC-LR standard solutions with different concentrations. Fig. 4A showed the SERS spectra of the MC-LR standard solution with different concentrations from 0.01 to 100 nM. It was observed that the signal intensities decreased with the increase of concentrations of MC-LR, meanwhile, the spectrum of the blank sample showed the strongest intensity. These results demonstrated the prominent specificity and affinity of aptamers toward the target MC-LR, which led to the specifically loss of the amplified signal within the hot spots that generated at the nanogaps of Au@AgNPs immobilized on the 3D-PSM and SERS nanotags. Moreover, it can also be seen in Fig. 4A that the signal of this SERS aptasensor was highly dependent on the concentration of MC-LR. The Raman peak at 1074 cm^{-1} was selected as the characteristic signal for MC-LR detection owing to its strongest intensity (as shown in Fig. 4A and B). In Fig. 4C, by plotting the SERS intensity at 1074 cm^{-1} versus the logarithm of the MC-LR concentration, a good linear correlation was obtained ranging from 0.01 to 100 nM. The regression equation was listed as $y = 4725.92–2102.75x$ (where y and x represented the SERS intensity at 1074 cm^{-1} and the logarithm of MC-LR concentration in nM, respectively) with a squared correlation coefficient of 0.9963. According to the IUPAC (International Union of Pure and Applied Chemistry) definition [35], the limit of detection (LOD, 3σ/m, as shown in S5) of this SERS aptasensor for MC-LR (at 1074 cm^{-1}) was found to be 7.8 pM (equal to ~156 amol), which showed higher sensitivity compared with the previously reported SERS sensing platform for MC-LR detection[28].

3.5. Specificity evaluation

The specific recognition ability of the sensor to the target was important to ensure the detection accuracy. The specificity of this 3D SERS aptasensor was investigated by detecting several potential interfering species including other microcystins (MC-YR and MC-RR), OTA, OTB and AFB1, each at a concentration of 100 nM. Fig. 5A showed the schematic demonstration of the specific recognition of MC-LR by the proposed 3D SERS aptasensor. Due to the high affinity and specificity against MC-LR, the MC-LR aptamer dissociated from the cDNA and consequently led to the release of SERS nanotags. Towards selective recognition of MC-LR, the specificity of the 3D SERS aptasensor (aptamer-based SERS sensor) and non-specific SERS sensor (ssDNA-based SERS sensor) were evaluated, respectively. As shown in Fig. 5B

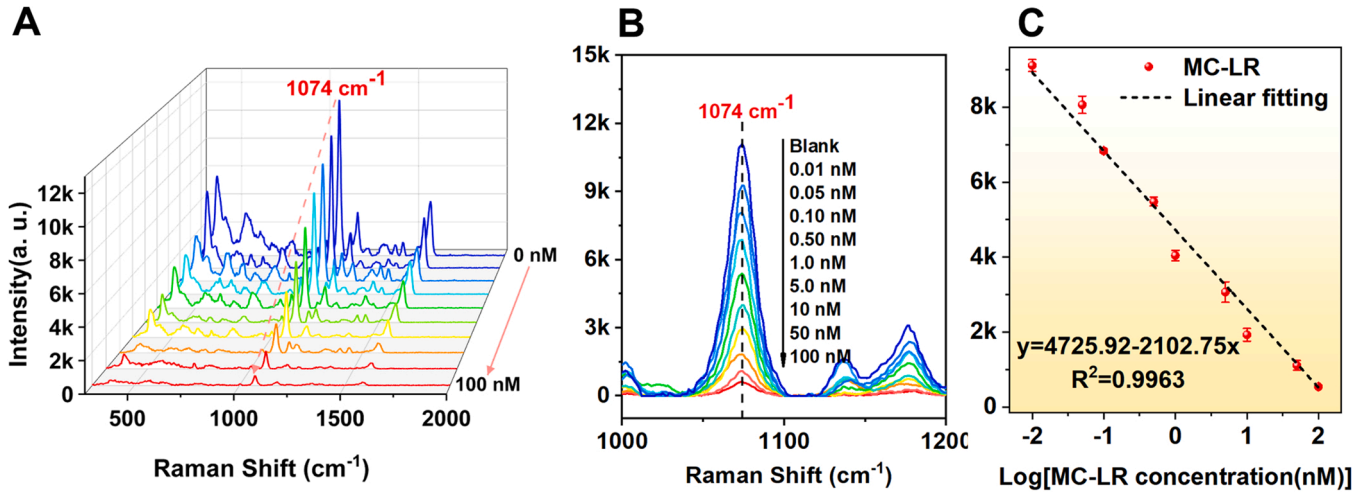


Fig. 4. SERS spectra of the SERS aptasensor in detection of MC-LR with different concentrations (0.01–100 nM) (A). The enlarged SERS spectra of SERS tags at different concentrations of MC-LR (B). The calibration curve of SERS intensity of SERS tags at 1074 cm^{-1} against the logarithm of different concentrations of MC-LR (C). Error bars were calculated based on the standard deviation of the average SERS intensity obtained by three repeated measurements.

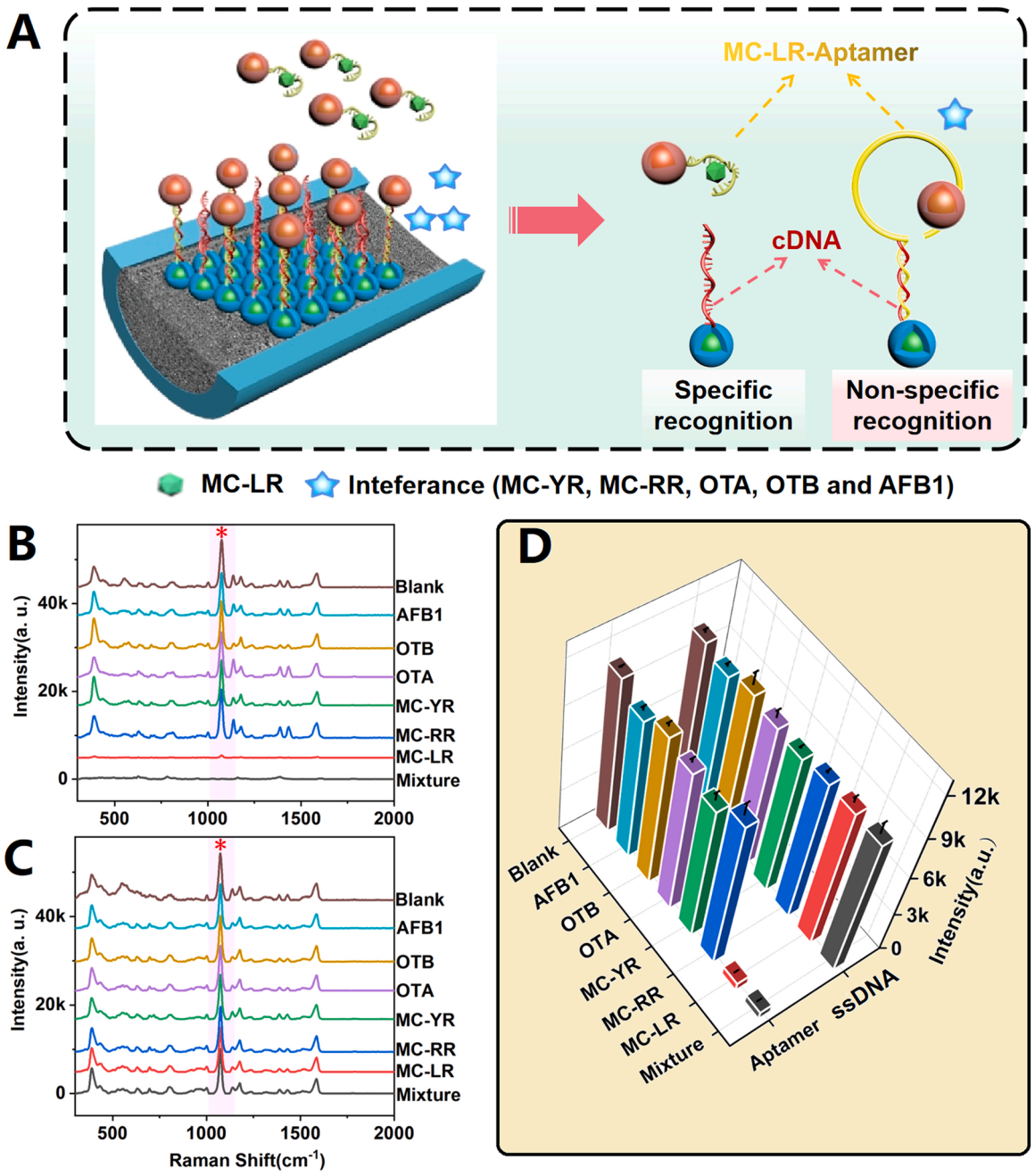


Fig. 5. Schematic demonstration of the specific recognition of MC-LR by the 3D SERS aptasensor (A). SERS spectra of the 3D SERS aptasensor (B) and a control ssDNA-modified SERS sensor (C) in the presence of 100 nM MC-LR, MC-RR, MC-YR, OTA, OTB and AFB1. Solvent blank was used as a negative control (Blank) and the mixture of all of the above samples was used as a control (Mixture). The corresponding histograms for the peak intensity at 1074 cm^{-1} (D).

and D, in contrast to a significant decrease in the SERS signals on exposure to the analyte of MC-LR, no obvious SERS signal variation compared to the blank were observed on exposure to the interfering species in the absence of MC-LR, which indicated that the 3D SERS aptasensor exhibited excellent specificity for MC-LR compared with other interfering species. However, for the non-specific SERS sensor, all of the analytes including MC-LR as well as other interfering species hardly caused an obvious signal change compared to the blank (as shown in Fig. 5C and D), which implied that the specific recognition could not be achieved by the ssDNA-based SERS sensor. This also confirmed the ability of our proposed platform for the high affinity and specific capture of MC-LR was achieved via interaction with the aptamers. Furthermore, when MC-YR, MC-RR, OTA, OTB and AFB1 were mixed in solution together with MC-LR (Mixture), the SERS intensity was almost the same as that of MC-LR (as shown in Fig. 5B and D). These results demonstrate that the proposed platform has the potential to be used for selective quantitative detection of MC-LR in complex matrix samples with high precision.

3.6. *Reproducibility and stability*

Fig. 6A1 and A2 showed the SERS spectra of hybridized SERS tags collected from 300 different points on a single SERS aptasensor and the corresponding heat map, respectively. It can be found that there were no obvious Raman intensity changes at the peak of 1074 cm^{-1}. Besides, the SERS signal reproducibility of the 3D SERS aptasensor was also investigated in terms of the relative standard deviation (RSD) of SERS intensity of SERS tags before and after MC-LR capturing. Fig. 6B1 and C1

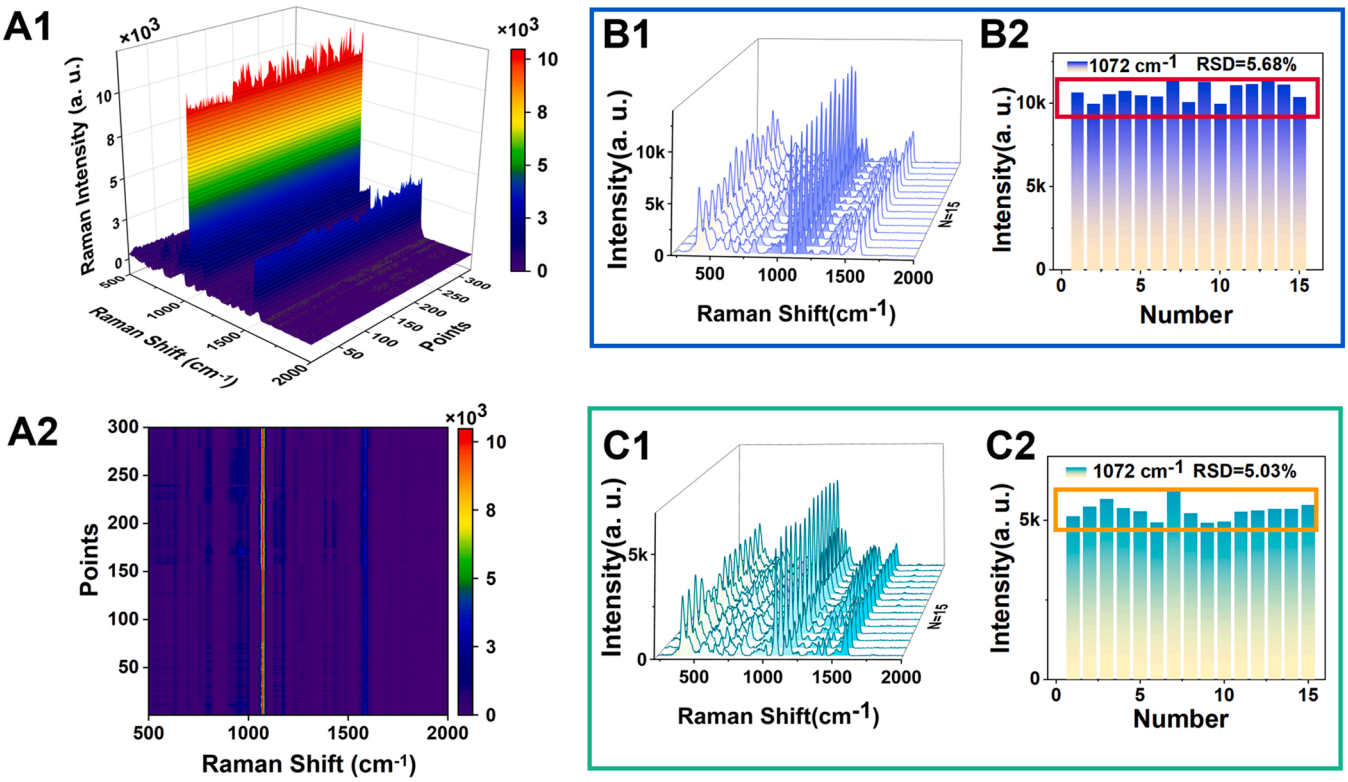


Fig. 6. Reproducibility and stability of the SERS aptasensor. SERS spectra of SERS tags collected from 300 different points on a single SERS aptasensor (A1) and the corresponding heat map (A2). SERS spectra of SERS tags acquired from 15 different spots on a single SERS aptasensor before (B1) and after (C1) percolating a volume of 20 μL of 0.50 nM MC-LR, and the corresponding histograms for the peak intensity at 1074 cm^{-1}, respectively (B2 and C2).

showed SERS spectra of tags acquired from 15 randomly selected spots on the 3D SERS aptasensor before and after MC-LR (0.50 nM) detection, respectively. And the corresponding histograms for the peak intensity at 1074 cm^{-1} were shown in Fig. 6B2 and Fig. 6C2, respectively. The RSD was respectively calculated to be 5.68 % and 5.03 %, which manifested satisfactory reproducibility. The stability of the SERS aptasensor prepared in the same batch (one-to-one) and different batches (batch-to-batch) were also investigated, respectively. As shown in Fig. S6 and Table S4, the one-to-one (n = 3) and batch-to-batch (n = 3) variations of the SERS intensity of tags at 1074 cm^{-1} peak were analyzed, and the RSD was calculated to be 3.55 ~ 3.75 %, and 4.50–5.33 %, respectively. Thereupon, this proposed SERS aptasensor revealed excellent signal homogeneity which could be applied as a reproducible SERS sensor for the quantitative specific analysis of MC-LR.

3.7. Practical application of the 3D SERS aptasensor

To demonstrate the applicability and practicability of the developed 3D SERS aptasensor, it was applied to the analysis of MC-LR in spiked tap-water and crucian carp samples. The aptasensors exhibited a sensitive SERS response to MC-LR with a wide range of concentrations from 0.01 nM to 100 nM (Fig. 7A1, B1). A progressive decrease of signal intensity occurred (1074 cm^{-1}) with the increasing amount of MC-LR. Fig. 7 A2, A3 and B2, B3 showed the relationship between the SERS signal of tags at peak position 1074 cm^{-1} and the concentration of MC-LR in spiked tap-water and crucian carp samples, respectively. A good linear relationship was observed and the squared correlation coefficient was high up to 0.9913 and 0.9922, respectively. The limit of detection (LOD, 3σ/m) was calculated to be 7.0 pM (equal to ~ 140 amol) for tap-water and 7.2 pM (equal to ~ 144 amol) for crucian carp samples, respectively. According to the equation shown in S6, the average recovery rates of MC-LR in the tap-water and crucian carp were calculated in the ranges of 94.1 ± 3.6 % ~ 102.4 ± 2.1 % and 94.6 ± 3.0 % ~ 103.6 ± 3.5 % (n = 3), respectively (Table S5).

In addition, as shown in Table S6, the capillary-based 3D aptasensor proposed in this work has the obvious advantages in sample consumption volume (20 μL) and specific recognition time (10 min) relative to the reported traditional solution-based or planar substrates [24,28, 36–39], owing to the substantially higher recognition and capture efficiency of the 3D-PSM and the unique structure of the capillary. The results indicated that this SERS aptasensor would be particularly potential and suitable for the quantitative specific analysis of MC-LR in real samples.

4. Conclusions

In summary, we proposed a novel 3D SERS aptasensor based on a porous silica network for the rapid detection and highly accurate quantification of trace MC-LR. The SERS aptasensor was prepared by immobilization of aptamer-modified SERS nanotags on the porous silica which was obtained by an in-situ polymerization of siloxane monomers in a quartz capillary via a facile method. The resulting formed unique hierarchically biporous structure coupled with aptamer could not only enable the rapid permeation of the aqueous phase but also provide high specific surface area and active sites, endowing the material with high capture efficiency of the target molecules. Besides, according to the size of aptamers, stable and uniformed hotspots of 7–8 nm in spacial size were formed, which precisely guaranteed the sensitivity, specificity, and stability of detection. The capillary-based 3D aptasensor served not only as a liquid flow channel, but also as a detection chamber. When liquid flow was pumped into the capillary channel, target molecules could be effectively enriched and captured in the "hot spot" regions, resulting in a higher capture and detection efficiency than conventional planar or solution-based SERS sensors. Furthermore, this SERS sensor platform features low sample consumption of only 20 μL per determination, fast analysis speed and easy to operate. The proposed aptasensor has

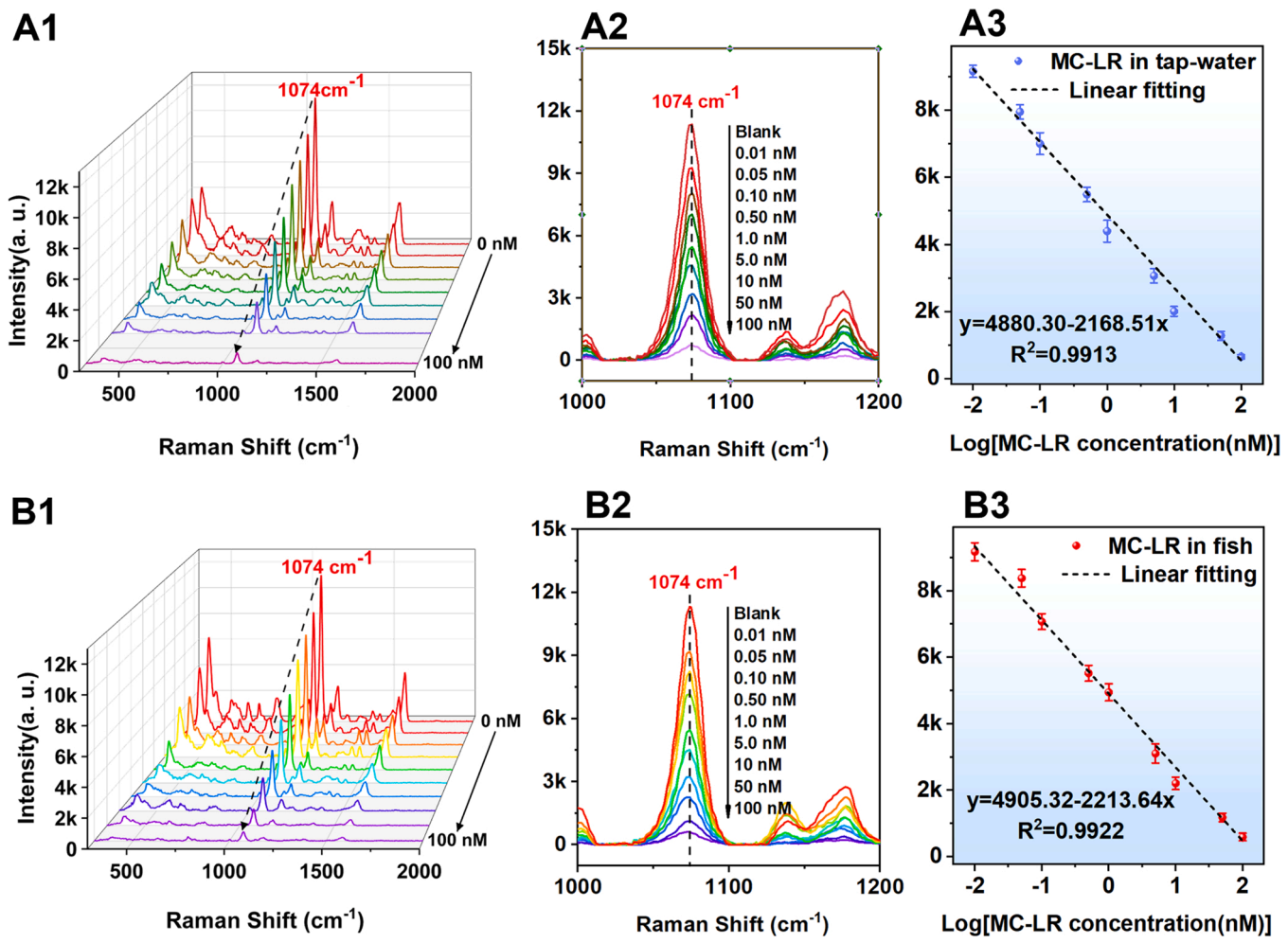


Fig. 7. SERS spectra of the tap-water (A1) and crucian carp fish (B1) with different concentrations of MC-LR (0.01–100 nM). The enlarged SERS spectra of SERS tags at different concentrations of MC-LR in tap-water (A2) and crucian carp fish (B2). The calibration curve of SERS intensity of SERS tags at 1074 cm^{-1} against the logarithm of different concentrations of MC-LR in tap-water (A3) and crucian carp fish (B3).

successfully accomplished quantitative determination of trace amounts of MC-LR in complex systems with a specific capture-release mode based on aptamer functionalized Au@Ag core-shell NPs. We also demonstrate that this platform has high sensitivity, high specificity, good reproducibility and satisfactory recovery. Therefore, we believe that this 3D SERS aptasensor is an alternative method for quick testing of trace amounts of hazardous substances and other fields of analysis related to public health and food/environmental security.

Declaration of Competing Interest

The authors declare that they have no known competing financial interests or personal relationships that could have appeared to influence the work reported in this paper.

Data Availability

Data will be made available on request.

Acknowledgements

This work was supported by Xiamen Youth Innovation Fund Project (3502Z20206063), Fujian Provincial Department of Education Young and Middle-aged Teachers Education Research Project (JAT210590, JAT210589).

Appendix A. Supporting information

Supplementary data associated with this article can be found in the online version at doi:10.1016/j.snb.2022.133248.

References

[1] H. Sun, S. Cong, Z. Zheng, Z. Wang, Z. Chen, Z. Zhao, Metal-organic frameworks as surface enhanced Raman scattering substrates with high tailorability, J. Am. Chem. Soc. 141 (2019) 870–878.
[2] Y. Cui, L. Xu, H. Li, X. Wang, F. Sun, H. Wang, et al., Flexible nano-cloth-like Ag cluster@rGO with ultrahigh SERS sensitivity for capture optimization-detection due to effective molecule–substrate interactions, Nanoscale 14 (2022) 12313.
[3] W. Fang, B. Zhang, F. Han, Z. Qin, Y. Feng, J. Hu, et al., On-site and quantitative detection of trace methamphetamine in urine/serum samples with a surface-enhanced Raman scattering-active microcavity and rapid pretreatment device, Anal. Chem. 92 (2020) 13539–13549.
[4] S. Kim, T. Kim, S. Lee, W. Kim, A. Bang, S. Moon, et al., Label-free surface-enhanced Raman spectroscopy biosensor for on-site breast cancer detection using human tears, ACS Appl. Mater. Interfaces 12 (2020) 7897–7904.
[5] J. Chi, C. Xia, Z. Guo, G. Huang, X. Lin, Gold nanoparticle-decorated porous silica for surface-enhanced Raman scattering-based detection of trace molecules in liquid phase, ACS Appl. Nano Mater. 5 (2022) 527–536.
[6] P. Zhao, H. Liu, L. Zhang, P. Zhu, S. Ge, J. Yu, Paper-based SERS sensing platform based on 3D silver dendrites and molecularly imprinted identifier sandwich hybrid for neonicotinoid quantification, ACS Appl. Mater. Interfaces 12 (2020) 8845–8854.
[7] Y. Zeng, S. Madsen, A. Yankovich, E. Olsson, R. Sinclair, Comparative electron and photon excitation of localized surface plasmon resonance in lithographic gold arrays for enhanced Raman scattering, Nanoscale 12 (2020) 23768–23779.

[8] J. Jeong, M. Arnob, K. Baek, S. Lee, W. Shih, Y. Jung, 3D Cross-point plasmonic nanoarchitectures containing dense and regular hot spots for surface-enhanced Raman spectroscopy analysis, Adv. Mater. 28 (2016) 8695–8704.
[9] R. Li, B. Gui, H. Mao, Y. Yang, D. Chen, J. Xiong, Self-concentrated SERS-active droplet sensor with threedimensional hot spots for highly sensitive molecular detection in complex liquid environments, ACS Sens. 5 (2020) 3420–3431.
[10] J. Li, H. Yan, X. Tan, Z. Lu, H. Han, Cauliflower-inspired 3D SERS substrate for multiple mycotoxins detection, Anal. Chem. 91 (2019) 3885–3892.
[11] N.J. Hao, P.Z. Liu, H. Bachman, Z. Chao, P.R. Zhang, J. Rufo, et al., Acoustofluidicsassisted engineering of multifunctional three-dimensional zinc oxide nanoarrays, ACS Nano 14 (2020) 6150–6163.
[12] A. San Juan, S. Chavva, D. Tu, M. Tircuit, G. Coté, S. Mabbott, Synthesis of SERS-active core-satellite nanoparticles using heterobifunctional PEG linkers, Nanoscale Adv. 4 (2022) 258–267.
[13] X. Xie, Y. Zhang, L. Zhang, J. Zheng, Y. Huang, H. Fa, Plasmon-driven interfacial catalytic reactions in plasmonic MOF nanoparticles, Anal. Chem. 93 (2021) 13219–13225.
[14] Y. Hong, M. Li, Z. Wang, B. Xu, Y. Zhang, S. Wang, et al., Engineered optoplasmonic core-satellite microspheres for SERS determination of methamphetamine derivative and its precursors, Sens. Actuators: B. Chem. 358 (2022), 131437.
[15] Y. Li, M. Guo, L. He, C. Huang, Y. Li, Green One-pot synthesis of silver nanoparticles/metal-organic gels hybrid and its promising SERS application, ACS Sustain. Chem. Eng. 7 (2019) 5292–5299.
[16] L. Wu, Y. Wang, X. Xu, Y. Liu, B. Lin, M. Zhang, et al., Aptamer-based detection of circulating targets for precision medicine, Chem. Rev. 121 (2021) 12035–12105.
[17] G. Huang, H. Zhao, P. Li, J. Liu, S. Chen, M. Ge, et al., Construction of optimal SERS hotspots based on capturing the spike receptor-binding domain (RBD) of SARS-CoV-2 for highly sensitive and specific detection by a fish model, Anal. Chem. 93 (2021) 16086–16095.
[18] Y. Wang, X. Du, X. Wang, T. Yan, M. Yuan, Y. Yang, et al., Patterned liquid-infused nanocoating integrating a sensitive bacterial sensing ability to an antibacterial surface, ACS Appl. Mater. Interfaces 14 (2022) 23129–23138.
[19] Y. Ye, X. Qi, H. Wang, B. Zhao, L. Xu, Y. Zhang, et al., A surface-enhanced Raman scattering aptasensor for Escherichia coli detection based on high-performance 3D substrate and hot spot effect, Anal. Chim. Acta 1221 (2022), 340141.
[20] L. Song, J. Li, H. Li, Y. Chang, S. Dai, R. Xu, et al., Highly sensitive SERS detection for Aflatoxin B1 and Ochratoxin A based on aptamer-functionalized photonic crystal microsphere array, Sens. Actuators: B. Chem. 364 (2022), 131778.
[21] Y. Hu, S. Giret, R. Meinusch, J. Han, F.-G. Fontaine, F. Kleitz, et al., Selective separation and preconcentration of Th(IV) using organo-functionalized, hierarchically porous silica monoliths, J. Mater. Chem. B 7 (2019) 289–302.
[22] J. Liu, I. White, D.L. DeVoe, Nanoparticle-functionalized porous polymer monolith detection elements for surface-enhanced Raman scattering, Anal. Chem. 83 (2011) 2119–2124.
[23] L. Ma, X. Zhao, Z. Zhang, H. Ge, J. Wang, A facile ultrasensitive detection of MC-LR toxin via a real-time assembled aptasensor of plasmonic graphene oxide, Talanta 236 (2022), 122864.
[24] X. Luo, X. Zhao, G. Wallace, M. Brunet, K. Wilkinson, P. Wu, et al., Multiplexed SERS detection of microcystins with aptamer-driven core-satellite assemblies, ACS Appl. Mater. Interfaces 13 (2021) 6545–6556.
[25] S. Eissa, M. Zourob, A graphene-based electrochemical competitive immunosensor for the sensitive detection of okadaic acid in shellfish, Nanoscale 4 (2012) 7593–7599.
[26] T. Pham, X. Vu, N. Dien, T. Trang, N. Truong, T. Thanh, et al., The structural transition of bimetallic Ag-Au from core/shell to alloy and SERS application, RSC Adv. 10 (2020) 24577.
[27] H. bin Pu, X. Xie, D. Suna, Q. Wei, Y. Jiang, Double strand DNA functionalized Au@Ag Nps for ultrasensitive detection of 17β-estradiol using surface-enhanced raman spectroscopy, Talanta 195 (2019) 419–425.
[28] Y. Zhao, F. Zheng, W. Ke, W. Zhang, L. Shi, H. Liu, Gap-tethered Au@AgAu Raman tags for the ratiometric detection of MC-LR, Anal. Chem. 91 (2019) 7162–7172.
[29] Yu Wang, K. Lee, J. Irudayaraj, SERS aptasensor from nanorod–nanoparticle junction for protein detection, Chem. Commun. 46 (2010) 613–615.
[30] A. Kaleem, M. Azmat, A. Sharma, G. Shen, X. Ding, Melamine detection in liquid milk based on selective porous polymer monolith mediated with gold nanospheres by using surface enhanced Raman scattering, Food Chem. 277 (2019) 624–631.
[31] N. Mhlanga, T. Domfe, A. Skepu, Fabrication of surface enhanced Raman spectroscopy substrates on solid supports, Appl. Surf. Sci. 476 (2019) 1108–1117.
[32] G. Liu, Y. Liu, L. Tang, X. Liu, G. Fu, Z. Liu, Semiconductor-enhanced Raman scattering sensors via quasi-three-dimensional Au/Si/Au structures, Nanophotonics 8 (2019) 1095–1107.
[33] O. Alsager, S. Kumar, G. Willmott, K. McNatty, J. Hodgkiss, Small molecule detection in solution via the size contraction response of aptamer functionalized nanoparticles, Biosens. Bioelectron. 57 (2014) 262–268.
[34] P. Privalov, C. Crane-Robinson, Translational entropy and DNA duplex stability, Biophys. J. 114 (2018) 15–20.
[35] A. Strickland, C. Batt, Detection of carbendazim by surface-enhanced Raman scattering using cyclodextrin inclusion complexes on gold nanorods, Anal. Chem. 81 (2009) 2895–2903.
[36] D. He, Z. Wu, B. Cui, Z. Jin, A novel SERS-based aptasensor for ultrasensitive sensing of microcystin-LR, Food Chem. 278 (2018) 197–202.
[37] Z. Zhang, J. Wang, Assembling of anisotropic plasmonic sheet-coresatellites for simultaneous ultrasensitive detection of MC-LR toxin, Analyst 146 (2021) 7005.
[38] B. Huo, L. Xia, Z. Gao, G. Li, Y. Hu, ATP-responsive strand displacement coupling with DNA origami/AuNPs strategy for the determination of microcystin-LR using surface-enhanced Raman spectroscopy, Anal. Chem. 94 (2022) 11889–11897.
[39] M. Li, S. Paidi, E. Sakowski, I. Barman, Ultrasensitive detection of hepatotoxic microcystin production from cyanobacteria using surface-enhanced Raman scattering immunosensor, ACS Sens. 4 (2019) 1203–1210.

Qian Xie received his Master's degree in 2015 from University of Toronto, Canada. He is currently an associate professor at Xiamen Huaxia University. His current scientific interests focused on the synthesis of capillary monolithic column and their applications in food safety and environmental monitoring.

Jinxin Chi received his Master's degree in applied chemistry from Fuzhou University in 2018. He then joined Xiamen Huaxia University, where currently he is working as a lecturer at the College of Environment and Public Health. His research interests include the synthesis of aptamer functionalized affinity monolithic column, as well as their applications in the area of environmental pollution and food analysis.

Zhixin Li obtained his B.S. degree from Huaqiao University in 2020. He is currently pursuing the Master's degree in Fuzhou University. His research focuses on the design and synthesis of functional nanomaterials and their applications for SERS sensors.

Xucong Lin received his Ph.D. degree in analytical chemistry from Fuzhou University in 2007. He is currently a professor at Fuzhou University. His research interests are in the area of environmental pollution and food analysis.

Guihua Huang received her Ph.D. degree in analytical chemistry from Fuzhou University in 2008. She is currently a professor at Xiamen Huaxia University. Her research focuses on the design and construction of plasmonic nanostructures for SERS sensing applications.